Author Manuscript

Author Manuscript

Author Manuscript

Author Manuscript

HHS Public Access

Author manuscript

Neuropharmacology. Author manuscript; available in PMC 2022 February 01.

Published in final edited form as:

Neuropharmacology. 2022 February 01; 203: 108885. doi:10.1016/j.neuropharm.2021.108885.

Sphingosine-1-phosphate receptor 1 agonist SEW2871 alters membrane properties of late-firing somatostatin expressing neurons in the central lateral amygdala

Briana E. Mork[a,c], **Sydney R. Lamerand**[d], **Shudi Zhou**[a,c], **Bradley K. Taylor**[d], **Patrick L. Sheets**[a,b,c,*]

[a] Medical Neurosciences Graduate Program, USA

[b] Department of Pharmacology and Toxicology, USA

[c] Stark Neurosciences Research Institute, Indiana University School of Medicine, Indianapolis, IN, 46202, USA

[d] Department of Anesthesiology and Perioperative Medicine, University of Pittsburgh School of Medicine, Pittsburgh, PA, 15213, USA

Abstract

Sphingosine-1-phosphate (S1P) is a bioactive sphingolipid that mediates a wide spectrum of biological processes including apoptosis, immune response and inflammation. Here, we sought to understand how S1P signaling affects neuronal excitability in the central amygdala (CeA), which is a brain region associated with fear learning, aversive memory, and the affective dimension of pain. Because the G-protein coupled S1P receptor 1 ($S1PR_1$) has been shown to be the primary mediator of S1P signaling, we utilized $S1PR_1$ agonist SEW2871 and $S1PR_1$ antagonist NIBR to determine a potential role of $S1PR_1$ in altering the cellular physiology of neurons in the lateral division of the CeA (CeL) that share the neuronal lineage marker somatostatin (Sst). CeL-Sst neurons play a critical role in expression of conditioned fear and pain modulation. Here we used transgenic breeding strategies to identify fluorescently labeled CeL-Sst neurons for electrophysiological recordings. Using principal component analysis, we identified two primary subtypes of Sst neurons within the CeL in both male and female mice. We denoted the two types regular-firing (type A) and late-firing (type B) CeL-Sst neurons. In response to SEW2871 application, Type A neurons exhibited increased input resistance, while type B neurons displayed a depolarized resting membrane potential and voltage threshold, increased current threshold, and

This is an open access article under the CC BY-NC-ND license (http://creativecommons.org/licenses/by-nc-nd/4.0/).

* Corresponding author. Indiana University School of Medicine, Neuroscience Research Building 400 D, 320 West 15th St, Indianapolis, IN 46202, USA. plsheets@iu.edu (P.L. Sheets).

CRediT authorship contribution statement

Briana E. Mork: Conceptualization, Methodology, Software, Formal analysis, Investigation, Writing, Visualization. **Sydney R. Lamerand:** Conceptualization, Methodology, Software, Formal analysis, Investigation, Writing, Visualization. **Shudi Zhou:** Formal analysis, Investigation. **Bradley K. Taylor:** Conceptualization, Methodology, Supervision, Project administration, Funding acquisition. **Patrick L. Sheets:** Conceptualization, Methodology, Writing, Supervision, Project administration, Funding acquisition.

Declaration of competing interest

The authors declare no competing financial interests.

Appendix A. Supplementary data

Supplementary data to this article can be found online at https://doi.org/10.1016/j.neuropharm.2021.108885.

Author Manuscript Author Manuscript Author Manuscript Author Manuscript

decreased voltage height. NIBR application had no effect on CeL Sst neurons, indicating the absence of tonic S1P-induced $S1PR_1$. Our findings reveal subtypes of Sst neurons within the CeL that are uniquely affected by $S1PR_1$ activation, which may have implications for how S1P alters supraspinal circuits.

Keywords

S1P; $S1PR_1$; Somatostatin; Central amygdala; Slice electrophysiology

1. Introduction

Sphingosine-1-phosphate (S1P) is a bioactive sphingolipid that mediates a wide spectrum of biological processes via five G protein-coupled S1P receptor subtypes ($S1PR_{1–5}$) (Alvarez et al., 2007; Lee et al., 1998). $S1PR_1$ is expressed ubiquitously in the body, with dominant expression over other S1P receptor subtypes (Coste et al., 2008; Strub et al., 2010). Incomplete vascular maturation and embryo death is observed in $S1PR_1^{-/-}$ mice, confirming the importance of $S1PR_1$ function for survival (Liu et al., 2000). Since its discovery in 1990, $S1PR_1$ has become increasingly of interest as a therapeutic target for treating multiple sclerosis, with various modulators already developed or in development (Chaudhry et al., 2017; Marciniak et al., 2018a; Quancard et al., 2012). While we know that S1PRs are expressed in multiple regions of the central nervous system (CNS), the functional organization of S1P pathways within specific brain regions are completely unknown. Currently, only a limited number of studies have examined S1P signaling in the CNS (Essis et al., 2015; Selley et al., 2013; Sim-Selley et al., 2009, 2018). Application of S1P and the $S1PR_1$ agonist SEW2871 evokes G-protein activity in the mouse amygdala (Sim-Selley et al., 2009; Waeber and Chiu, 1999).

The central nucleus of the amygdala (CeA) encompasses the main output pathways of the amygdala. Numerous studies, including from our laboratory, report variability in the electrophysiological and molecular identity of CeA neurons (Dumont et al., 2002; Haubensak et al., 2010; Hunt et al., 2017; Li and Sheets, 2018; Penzo et al., 2014; Schiess et al., 1999). Molecular identity of CeA neurons is associated with distinct functional roles in circuits and behavior (Haubensak et al., 2010; McCall et al., 2015; Penzo et al., 2014). For instance, protein kinase C-δ (pKCδ) is expressed in a ‘late-firing’ neurons in the central lateral (CeL) amygdala, and inhibition of these pKCδ+ neurons facilitates fear expression (Ciocchi et al., 2010; Haubensak et al., 2010). Activation of neighboring CeL neurons expressing somatostatin (Sst), which have negligible overlap with pKCδ+ neurons, induces freezing behavior associated with the fear response (Li et al., 2013).

Extensive research has also shown that CeA neurons are sensitized in models of both inflammatory (Ji et al., 2009; Ji and Neugebauer, 2007; Li and Neugebauer, 2004a, b; Neugebauer and Li, 2003; Sosulina et al., 2006) and neuropathic pain (Goncalves and Dickenson, 2012). Therefore, the CeA has been termed the ‘nociceptive amygdala’ (Neugebauer, 2015). Evidence shows that chemogenetic activation of Sst neurons and inhibition of pKCδ+ CeA neurons reduces pain behavior caused by peripheral nerve injury

Author Manuscript Author Manuscript Author Manuscript Author Manuscript

(Wilson et al., 2019). Conversely, recent work showed that general anesthetics can reduce neuropathic pain behavior via activation of CeA pKCδ+ neurons (Hua et al., 2020). This body of work delineates the importance of understanding the functional effects of S1P signaling in defined cell-types in the CeA. Here we used transgenic breeding strategies to fluorescently label neurons that share the neuronal lineage marker Sst in the CeL (CeL-Sst neurons) and target them for electrophysiological recordings in acute brain slices. Our goal was to determine the effects of the $S1PR_1$ agonist SEW2871 and $S1PR_1$ antagonist NIBR on subthreshold and suprathreshold excitable properties of CeL-Sst neurons.

2. Materials and methods

2.1. Animals

To generate transgenic offspring expressing the red fluorescent protein Td-Tomato specifically in neurons that share the neuronal lineage marker Sst, female B6N.Cg-*Sst*$^{tm2.1(Cre)Zjh/J}$ (Jackson Laboratories, RRID:IMSR_JAX:018973) mice were mated with male B6.Cg-*Gt(ROSA)26Sor*$^{tm14(CAG-tdTomato)Hze/J}$ mice (Jackson Laboratories, RRID:IMSR_JAX:007909). We refer to these transgenic offspring as Sst-Cre; Ai14 mice in this manuscript, total n = 89 (50 female, 39 male). Mice were used in accordance with the animal care and use guidelines of Indiana University, the National Institutes of Health, and the Society for Neuroscience.

2.2. Slice preparation

Brain slices were prepared as previously described (Li and Sheets, 2018). Slices at postnatal days 30–95 (mean, 51.5; mode, 42; median, 48) were used for component analysis (Methods 2.5) and slices at postnatal days 28–64 (mean, 50.8; mode, 39; median, 53) were used for pharmacology experiments. Coronal slices (300 μm thick) containing amygdala were made by vibratome-sectioning the brain (VT1200S, Leica) in chilled cutting solution (composed of, in mM: 110 choline chloride, 25 $NaHCO_3$, 25 D-glucose, 11.6 sodium ascorbate, 7 $MgSO_4$, 3.1 sodium pyruvate, 2.5 KCl, 1.25 NaH_2PO_4, and 0.5 $CaCl_2$). Slices were transferred to artificial cerebrospinal fluid (ACSF, composed of, in mM: 127 NaCl, 25 $NaHCO_3$, 25 D-glucose, 2.5 KCl, 1 $MgCl_2$, 2 $CaCl_2$, and 1.25 NaH_2PO_4, aerated with 95% O_2/5% CO_2) at 37 °C for 30 min. Slices were subsequently incubated at room temperature (~21 °C) in ACSF for at least 1 h prior to electrophysiological recordings.

2.3. Electrophysiology

Coronal brain slices containing the CeA were transferred to the recording chamber of an upright microscope (BX51, Olympus), and held in place with short pieces of flattened gold wire (0.813 mm diameter; Alfa Aesar). We targeted fluorescently labeled neurons in the right CeA that were visualized using coolLED optics (Scientifica). Recordings were targeted to the CeL subdivision of the CeA; however, a small fraction may have been from CeC. Pipettes for recordings were fabricated from borosilicate capillaries with filaments (G150-F, Warner) using a horizontal puller (P-97, Sutter). For acquiring the electrophysiological profiles of td-Tomato positive neurons, patch pipettes contained potassium-based intracellular solution (in mM: 128 K-gluconate, 10 HEPES, 1 EGTA, 4 $MgCl_2$, 4 ATP, and 0.4 GTP, 10 phosphocreatine, 3 ascorbate; pH 7.2). EGTA was

Author Manuscript Author Manuscript Author Manuscript Author Manuscript

included both to facilitate seal formation and to reduce cytosolic calcium elevations induced by the various stimulus protocols used in these studies. Slices were ideally used 1.5–3 h after preparation, but some were used up to 4 h after preparation. Whole-cell patch-clamp recordings of neuron properties were performed in recirculating ACSF containing synaptic blockers (in mM: 5 CPP, 10 NBQX, 5 GABAzine). The recording temperature was controlled by an in-line heating system (TC324B, Warner) that warmed recirculating ACSF prior to entering the recording chamber. Recordings were performed at 29–32 °C and the ACSF was refreshed with each new slice. Pipette capacitance was compensated; series resistance was monitored but not compensated and required to be < 30 MΩ for inclusion in the data set. Current-clamp recordings were bridge-balanced. Recordings were filtered at 4 kHz and sampled at 10 kHz using a Multiclamp 700B amplifier (Molecular Devices). Membrane potential values were not corrected for a calculated liquid junction potential of 11 mV. Ephys software (http://www.ephus.org) was used for data collection (Suter et al., 2010). Cells that exhibited series resistance >30 MΩ were excluded from analysis. Cells that had less than the greater value of 2 MΩ or 15% change in series resistance before and after drug application were excluded from pharmacology analysis. Methods for determining input resistance and voltage threshold for action potential (AP) firing have been reported previously (Suter et al., 2013). Briefly, input resistance was measured as the slope of a linear least-squares fit to the voltage-current relationship established from steady-state responses to a series of hyperpolarizing and subthreshold depolarizing current steps (duration 1.0 s, amplitude ≤100 pA). The voltage threshold for AP firing was calculated as the point where *dV/dt* exceeded 10% of its maximum value relative to the mean *dV/dt* baseline measured over the 4–5 msec window before the AP peak. Frequency-current slope was calculated using a polynomial fit to the firing frequency at current threshold through the firing frequency at twice the current threshold.

2.4. Pharmacological agents

5-[4-phenyl-5-(trifluoromethyl)-2-thienyl]-3-[3-(trifluoromethyl)phenyl]-1,2,4-oxadiazole (SEW2871, $S1PR_1$ agonist) was purchased from Cayman Chemical (Ann Arbor, MI). SEW2871 displays an EC_{50} = 13 ± 8 for $S1PR_1$ with no interaction at a concentration of 10 μM with $S1PR_{2–5}$ in cell culture (Marciniak et al., 2018b). (S)-2-(3′-[(R)-1-((4-Chloro-3-methyl-phenyl)-ethylamino]-3,5-dimethyl-biphenyl-4-carbonyl)-amino)-propionic acid, N-[[3′-[[(1R)-1-(4-Chloro-3-methylphenyl)ethyl]amino]-3,5-dimethyl[1,1′-biphenyl]-4-yl]carbonyl]-L-alanine (NIBR-0123), competitive $S1PR_1$-selective antagonist) was purchased from Sigma-Aldrich (St. Louis, MO) and made according to manufacturer-provided data sheet: dissolved into di-methyl sulfoxide (DMSO) for stock solutions of [2 mM]. NIBR-0123 is specific to $S1PR_1$ with an IC_{50} of 2.5 nM. No internalization of the receptor was observed up to 100 μM (Quancard et al., 2012). The final solution of SEW2871 [100 nM] and NIBR [100 nM] used in electrophysiological recordings was made by diluting stock solutions directly into ACSF during recordings. All other reagent grade chemicals were purchased from Sigma-Aldrich (St. Louis, MO) or Thermo Fisher Scientific (Waltham, MA).

Author Manuscript Author Manuscript Author Manuscript Author Manuscript

2.5. Data analysis

Principal component analysis (PCA) was performed on CeL Sst neurons using the following input parameters at resting membrane potential: time of first inter-spike interval (PC1), time to first spike (PC2), current threshold (PC3), action-potential half-width (PC4), frequency-current slope (PC5), and input resistance (PC6). This technique reduces the number of variables in a large data set while retaining much of the information in the original data set, reducing the dimensions by finding linear combinations of data. After the data is standardized, principal components are determined by component variance and data is grouped by ward linkage. Principal components and associated eigenvalue, percent explained: PC1 (2.04, 34%), PC2 (1.26, 21%), PC3 (1.06, 17.7%), PC4 (0.864, 14.4%), PC5 (0.528, 8.8%), PC6 (0.247, 4.11%). Three-way ANOVA statistical analysis of Sst subtype differences was conducted using GraphPad Prism 8 (San Diego, CA). GraphPad Prism 8 was used for mixed-effect statistical analyses of each drug treatment in pharmacology experiments presented in Figs. 4–6, Table 2. For statistical analyses of pre-treated pharmacology experiments (Fig. 7, Table 3), a Lilliefors test was performed prior to significance testing to determine if the data were normally distributed. Pairwise comparisons between groups were performed with the Student's paired *t*-test (for normally distributed data) or the Wilcoxon rank sum test (for non-normally distributed data). Error bars in plots represent standard error of the mean (SEM).2.6 Fluorescence *in situ* hybridization.

Sst-Cre; Ai14 mice were deeply anesthetized with an overdose of pentobarbital (100 mg kg^{-1}, 0.2 mL i.p. Fatal-Plus, Henry Schein, Melville, NY, USA) or a mixture of ketamine (80 mg/kg) and xylazine (12 mg/kg; i.p.), respectively, and then transcardially perfused with 1X phosphate buffered saline (PBS; pH 7.4) followed by 10% buffered formalin. Brains were extracted, post-fixed in 10% formalin 2–4 h at 4 °C, and then stored in 30% sucrose at 4 °C. Coronal brain sections (20 μm) were obtained on a vibrating microtome and mounted on Superfrost Plus Microscope slides (Thermo Fisher Scientific, Waltham, MA, USA). Pretreatment for fluorescence *in situ* hybridization (FISH) consisted of bathing slides in Xylene for 10 min and 100% ethanol for 4 min. Slides were washed in deionized H_2O and allowed to dry overnight. The following day the FISH protocol for RNAscope Fluorescent v2 Assay (Advanced Cell Diagnostics) was followed for hybridization to marker probes (RNAscope® Probe- Mm-S1PR1, 426001; RNAscope® Probe-Mm-Sst-C2, 404631-C2) at 40 °C in a HybEZ oven. Following amplification and labeling steps per manufacturer's instructions, slides were washed in PBS, then air dried and cover slipped with Vectashield antifade mounting medium with 4′,6-diamidino-2-phenylindole (DAPI) (Vector Labs, Burlingame, CA, USA). All images were captured on a Nikon (Tokyo, Japan) Eclipse Ti2 microscope using a 40x objective. The same exposure time was used for all images captured in each channel, and each image composed of 64 individual exposures (8 × 8) stitched together with 10% overlap. Image capture, adjustments and quantification were performed in NIS-Elements Advanced Research software v5.02.

For quantification of FISH, a cell was deemed to express somatostatin (Sst) and/or $S1PR_1$ mRNA when at least four fluorescent puncta were observed, with a DAPI-counterstained nucleus visible. Delineations of the CeA and its subdivisions (CeM, CeC, CeL) were identified according to Paxinos and Franklin (2013). The number of SOM mRNA expressing

Author Manuscript Author Manuscript Author Manuscript Author Manuscript

cells were counted in each area of the CeA. Each Sst mRNA expressing cell was then evaluated for $S1PR_1$ expression. Sections (4–5) were counted per mouse and averaged with *n* defined as one mouse. Results are presented as mean ± SEM. Data were analyzed using GraphPad Prism 9 (GraphPad Software Inc., USA).

3. Results

3.1. The CeL contains intrinsically distinct Sst neurons subtypes

We targeted tdTomato-expressing neurons in the right CeL (CeL Sst neurons) for whole-cell electrophysiological recordings in acute brain slices from Sst-Cre; Ai14 tdTom mice (Fig. 1A–D). Using principal component analysis (section 2.5) of recording data from 72 neurons at resting membrane potential (RMP), we found that there are two intrinsically distinct subtypes of CeL Sst neurons. The slightly predominant CeL Sst phenotype “type A” (41 out of 72) displayed an early onset of action potential (AP) firing in response to a depolarizing current step (500 msec) compared to the delayed AP onset (‘late-firing’) of the other CeL Sst phenotype “type B” (31 out of 72; Fig. 2A, C). Smaller amplitude of injected current was needed to evoke APs in type A neurons (Fig. 2B and C). We found that type A neurons, compared to type B neurons, are significantly more depolarized, have a narrower action potential half-width, and decreased spike frequency adaptation (Fig. 2C, Table 1). Spike frequency adaptation is a firing behavior which increases the threshold for subsequent spikes in a series of action potentials, regulated by ion channels including voltage-gated K^+/KCNQ channels (Santini and Porter, 2010; Watanabe et al., 2017). These type A and type B intrinsic phenotypes have been described previously in the CeL (Amano et al., 2012; Haubensak et al., 2010; Li and Sheets, 2018) including within CeL Sst populations (Hunt et al., 2017). While we observed a small population of spontaneously firing CeL Sst neurons (n = 4), characterized in previous studies (Adke et al., 2021; Wilson et al., 2019), we excluded these cells from analyses and pharmacological experiments.

We compared intrinsic properties of CeL Sst subtypes in male and female mice, which revealed a significant main effect of cell type for factors including RMP, current threshold, voltage threshold, spike frequency adaptation and time to first spike. The only observed effect of sex was decreased voltage threshold in female cells, however no significant effect of interaction between sex and cell type for any properties was observed (3-way ANOVA: Table 1). Finally, we compared the action potential (AP) frequency-current (FI) relationship, which compares AP frequency in response to injected step current, in type A and type B cells, in male and female mice (Fig. 3A–C). We found a significant effect of cell type and interaction (current x cell type), and no effect of sex (3-way rmANOVA: Fig. 3). Because of this, we collapsed across sex for studying $S1PR_1$ pharmacology in CeL Sst subtypes.

3.2. The $S1PR_1$ agonist SEW2871 differentially alters the intrinsic membrane properties of CeL Sst subtypes

Bath application of SEW2871 [100 nM] for 10 min did not alter the RMP or the FI relationship of type A CeL Sst neurons (Fig. 4A–C, Table 2). We also did not observe any significant changes to firing properties measured in type A neurons after SEW2871 application (Table 2). The vehicle for SEW2871 DMSO had no effect on RMP, input

Author Manuscript Author Manuscript Author Manuscript Author Manuscript

resistance, FI relationship, or any other firing properties of type A neurons (Fig. 4D–F, Table 2). In contrast to type A neurons, SEW2871 significantly depolarized RMP and increased input resistance of type B CeL Sst neurons (Fig. 5A–B, Table 2). SEW2871 significantly depolarized voltage threshold for AP firing and decreased both voltage height of APs and time to first AP in type B neurons (Table 2). Surprisingly, SEW2871 application did not alter FI relationship of type B neurons (Fig. 5C, Table 2). As observed in type A neurons, DMSO had no effect the sub-threshold and firing properties of type B neurons with the exception of significantly reducing spike-frequency adaptation (Fig. 5D–F, Table 2). This was a surprising finding in that we did not observe changes to spike-frequency adaptation following SEW application (Table 2).

3.3. The competitive antagonist for $S1PR_1$ NIBR did not alter RMP or FI relationship in either subtype of CeL Sst neurons

We next tested whether there was tonic S1P-induced activity of $S1PR_1$ in CeL Sst neurons using the $S1PR_1$ antagonist NIBR [100 nM]. We found that bath application of NIBR for 10 min did not significantly change any measured intrinsic properties for type A neurons with the exception of reducing the FI slope (Fig. 6A–C, Table 2). Application of NIBR had no significant effect on RMP or FI relationship of type B CeL Sst neurons (Fig. 6D–F, Table 2). These findings indicate that there is limited or no tonic S1P-induced $S1PR_1$ activity in CeL slice recordings of type A and type B CeL Sst neurons.

3.4. NIBR blocks the depolarizing effects of SEW2871 on type B CeL Sst neurons

We next asked whether NIBR blocked the effects of SEW2871 on type B CeL Sst neurons. NIBR was added to the bath and baseline values were recorded after approximately 7 min to allow time for equilibrium and adequate antagonism of $S1PR_1$. Subsequent bath application of SEW2871 for 10 min did not alter any subthreshold or firing properties of type B CeL Sst neurons (Fig. 7A–C, Table 3). These data suggest that the intrinsic changes induced by SEW2871 on type B CeL Sst neurons is due to activation of $S1PR_1$.

3.5. Only a subset of CeL Sst neurons express $S1PR_1$ mRNA

We next performed fluorescent *in situ* hybridization (Methods 2.6) to determine expression of $S1PR_1$ mRNA in tdTomato-expressing CeL neurons (Fig. 8A–B). We found that co-expression of SOM (RNAscope probe) and tdTom in the CeL was not 100% (average 39.0 ± 8.6%; Fig. 8C), with significantly higher co-expression in male mice (average 51.7%, n = 2 animals, 4–5 slices averaged per animal) than female mice (average 26.3%, n = 2 animals, 4–5 slices averaged per animal). Of note, co-expression of $S1PR_1$ and SOM (41.5 ± 6.0%; Fig. 8C) was higher than co-expression of $S1PR_1$ and tdTomato (33.6 ± 3.0%; Fig. 8C). Less than half of tdTomato-expressing CeL neurons were positive for both SOM and $S1PR_1$ (41.4 ± 7.3%; Fig. 8C). These data show that $S1PR_1$ mRNA is detected in a subset of CeL neurons from Sst-Cre; Ai14 mice expressing both Sst mRNA and td-Tomato.

4. Discussion

Using whole cell electrophysiology in acute brain slice, we confirmed two distinct cell subtypes of CeL Sst neurons, consistent with previously identified firing phenotypes of CeL

Author Manuscript Author Manuscript Author Manuscript Author Manuscript

Sst subtypes (Hunt et al., 2017; Wilson et al., 2019). Intrinsic differences between type A and type B neurons were consistent for male and female mice. Using FISH, we found that Sst mRNA is detected in approximately half of the td-Tomato expressing neurons within the right CeA. In the motor cortex with a more limited number of Sst neurons, we observed a nearly complete overlap of Sst mRNA and td-Tomato expression (Supplemental Fig. 1). This suggests that Sst expression in the CeA diminishes during development. Currently, we cannot specify whether the incomplete overlap in Sst mRNA and td-Tomato expression in the CeL contributes to the intrinsic differences observed between type A and type B neurons. Disparities in the functional roles of the type A and type B Sst neuron subtypes in the CeL remain to be determined. Previous work has shown that CeL Sst neurons send projections to the periaqueductal gray (PAG), a midbrain structure essential to both fear and pain processing (Penzo et al., 2014). Work from our laboratory found that different firing phenotypes of CeA neurons project to distinct subregions within the PAG (Li and Sheets, 2018), and these subregions have been shown to regulate specific behaviors associated with fight-or-flight responses and endogenous analgesia mechanisms (Bandler and Carrive, 1988; Bandler and Depaulis, 1988; LeDoux et al., 1988). Additional work revealed that CeL Sst neurons send local inputs that control the firing of both neighboring Sst-positive and Sst-negative neurons within the CeL (Hunt et al., 2017). This suggests that type A and type B CeL Sst neurons may have different local and long-range anatomical targets that mediate unique components of amygdala processing and output, including modulation of pain and fear.

Currently, the complexity of supraspinal circuits and the wide distribution of S1PRs in the CNS make it difficult to understand the short- and long-term effects of S1P signaling on brain function. Previous studies confirm that $S1PR_1$ ligands cross the blood brain barrier (Foster et al., 2007; Yanagida et al., 2017), and engage receptors throughout the brain (Sim-Selley et al., 2009; Welch et al., 2012) including within the amygdala. Therefore, understanding S1P signaling in supraspinal pathways is critical for developing therapeutic strategies that deliver S1PR ligands to the brain. Here our work provides new insight into how $S1PR_1$ activation affects the activity of a specific population of amygdala neurons known to be involved in both pain and fear modulation. Specifically, we show that the $S1PR_1$ agonist SEW2871 depolarizes the resting membrane potential for type B, but not type A, CeL Sst neurons. Typically, depolarization of membrane potential and increased input resistance is associated with increased excitability as it pushes a neuron closer to threshold for AP firing. However, we found that AP frequency in response to depolarizing current steps was unchanged in type B CeL Sst neurons after SEW2871 application. In addition, SEW2871 depolarized voltage threshold for AP firing and reduced voltage height in type B CeL Sst neurons. These findings suggest that $S1PR_1$ activation decreases the excitability of type B CeL Sst neurons. The $S1PR_1$ antagonist NIBR blocked the effects evoked by SEW2871 indicating expression of $S1PR_1$ in type B CeL Sst neurons. This is consistent with our FISH data showing detection of $S1PR_1$ mRNA in approximately 34% of td-Tomato expressing neurons in the CeL, which is similar to the number of type B CeL Sst neurons we detected electrophysiologically (~43%). Therefore, we conclude the observed effects of SEW2871 were due to activation of $S1PR_1$ expressed in type B CeL Sst neurons.

Author Manuscript Author Manuscript Author Manuscript Author Manuscript

Neuronal depolarization observed after SEW2871 application suggests that $S1PR_1$ signaling is altering the activity of membrane ion channels. One possible mechanism responsible for our findings is that $S1PR_1$ activation leads to closure or inhibition of an ion channel that is active near RMP of the cell. There are numerous possibilities for the effectors of $S1PR_1$ signaling including KCNQ potassium channels, which are present in the amygdala (KCNQ3, KCNQ5) (Lein et al., 2007; Science, 2006). $S1PR_1$ activation has been shown to stimulate phospholipase C (PLC) (Alewijnse et al., 2004), which is known to suppress KCNQ activity via reduction of PIP_2 levels (Delmas and Brown, 2005; Okamoto et al., 1998; Suh and Hille, 2007). Other evidence suggests that S1P can activate transient receptor potential (TRP) channel subtype 5 (E et al., 2011; Xu et al., 2006), which is expressed in the amygdala (Riccio et al., 2009). Recent work identified voltage-gated chloride channels, CLCN3 and CLCN5, as responsible for S1P-induced excitatory conductance and membrane depolarization in sensory neurons (Qi et al., 2018). Finally, S1P has been shown to induce intracellular Ca^{2+} mobilization (Meyer zu Heringdorf et al., 2001), suggesting that the depolarization of type B CeL Sst neurons by SEW2871 may involve increases in intracellular Ca^{2+} concentrations.

Our results do not exclude the possibility that astrocytic $S1PR_1$ activation leads to astrocyte-mediated modulation of CeL Sst neurons. Previous reports show that $S1PR_1$ is localized to astrocytes in the CNS (Chen et al., 2019; Choi et al., 2011; Nishimura et al., 2010). Upregulation of astrocytic $S1PR_1$ and $S1PR_3$ is observed in brain lesions of multiple sclerosis patients (Van Doorn et al., 2010). Importantly, $S1PR_{1,3-5}$ ligand fingolimod improved clinical scores in a mouse model of multiple sclerosis, which was ineffective in mice lacking $S1PR_1$ on GFAP-expressing astrocytes, but not on neurons (Choi et al., 2011). Additional investigation into the role of S1P on astrocyte-neuron signaling within the CeL is needed for a complete understanding of how endogenous S1P alters cellular activity in supraspinal circuits.

5. Conclusions

Overall, our results confirmed that CeL Sst neurons are a heterogeneous population of intrinsically distinct neurons that are differentially affected by the $S1PR_1$ agonist SEW2871. These findings provide the first evidence for $S1PR_1$ signaling altering the intrinsic properties of molecularly and physiologically distinct subset of neurons in the CeL. We also provide evidence showing that $S1PR_1$ is expressed in subset of CeL Sst neurons, which provides insight into S1P signaling that may alter the activity of specific neurons in the CeL.

Supplementary Material

Refer to Web version on PubMed Central for supplementary material.

Acknowledgements

We would like to thank Dr. Andrea F. Jones for mouse generation and laboratory support. We would like to thank Tyler J. McCray for assistance and support.

Author Manuscript Author Manuscript Author Manuscript Author Manuscript

Funding

This work was supported by the National Institutes of Health [grant number R01-NS112632].

References

Adke AP, Khan A, Ahn HS, Becker JJ, Wilson TD, Valdivia S, Sugimura YK, Martinez Gonzalez S, Carrasquillo Y, 2021. Cell-type specificity of neuronal excitability and morphology in the central amygdala. eNeuro 8.

Alewijnse AE, Peters SL, Michel MC, 2004. Cardiovascular effects of sphingosine-1-phosphate and other sphingomyelin metabolites. Br. J. Pharmacol. 143, 666–684. [PubMed: 15504747]

Alvarez SE, Milstien S, Spiegel S, 2007. Autocrine and paracrine roles of sphingosine-1-phosphate. Trends Endocrinol. Metabol. 18, 300–307.

Amano T, Amir A, Goswami S, Pare D, 2012. Morphology, PKCdelta expression, and synaptic responsiveness of different types of rat central lateral amygdala neurons. J. Neurophysiol. 108, 3196–3205. [PubMed: 22972957]

E AL-S, Tumova S, Naylor J, Majeed Y, Li J, Beech DJ, 2011. GVI phospholipase A2 role in the stimulatory effect of sphingosine-1-phosphate on TRPC5 cationic channels. Cell Calcium 50, 343–350. [PubMed: 21742378]

Bandler R, Carrive P, 1988. Integrated defence reaction elicited by excitatory amino acid microinjection in the midbrain periaqueductal grey region of the unrestrained cat. Brain Res. 439, 95–106. [PubMed: 3359200]

Bandler R, Depaulis A, 1988. Elicitation of intraspecific defence reactions in the rat from midbrain periaqueductal grey by microinjection of kainic acid, without neurotoxic effects. Neurosci. Lett. 88, 291–296. [PubMed: 3386876]

Chaudhry BZ, Cohen JA, Conway DS, 2017. Sphingosine 1-phosphate receptor modulators for the treatment of multiple sclerosis. Neurotherapeutics 14, 859–873. [PubMed: 28812220]

Chen Z, Doyle TM, Luongo L, Largent-Milnes TM, Giancotti LA, Kolar G, Squillace S, Boccella S, Walker JK, Pendleton A, Spiegel S, Neumann WL, Vanderah TW, Salvemini D, 2019. Sphingosine-1-phosphate receptor 1 activation in astrocytes contributes to neuropathic pain. Proc. Natl. Acad. Sci. U. S. A. 116, 10557–10562. [PubMed: 31068460]

Choi JW, Gardell SE, Herr DR, Rivera R, Lee CW, Noguchi K, Teo ST, Yung YC, Lu M, Kennedy G, Chun J, 2011. FTY720 (fingolimod) efficacy in an animal model of multiple sclerosis requires astrocyte sphingosine 1-phosphate receptor 1 (S1P1) modulation. Proc. Natl. Acad. Sci. U. S. A. 108, 751–756. [PubMed: 21177428]

Ciocchi S, Herry C, Grenier F, Wolff SB, Letzkus JJ, Vlachos I, Ehrlich I, Sprengel R, Deisseroth K, Stadler MB, Muller C, Luthi A, 2010. Encoding of conditioned fear in central amygdala inhibitory circuits. Nature 468, 277–282. [PubMed: 21068837]

Coste O, Brenneis C, Linke B, Pierre S, Maeurer C, Becker W, Schmidt H, Gao W, Geisslinger G, Scholich K, 2008. Sphingosine 1-phosphate modulates spinal nociceptive processing. J. Biol. Chem. 283, 32442–32451. [PubMed: 18805787]

Delmas P, Brown DA, 2005. Pathways modulating neural KCNQ/M (Kv7) potassium channels. Nat. Rev. Neurosci. 6, 850–862. [PubMed: 16261179]

Dumont EC, Martina M, Samson RD, Drolet G, Pare D, 2002. Physiological properties of central amygdala neurons: species differences. Eur. J. Neurosci. 15, 545–552. [PubMed: 11876782]

Essis SA, Laurier-Laurin ME, Pepin E, Cyr M, Massicotte G, 2015. GluN2B-containing NMDA receptors are upregulated in plasma membranes by the sphingosine-1-phosphate analog FTY720P. Brain Res. 1624, 349–358. [PubMed: 26260438]

Foster CA, Howard LM, Schweitzer A, Persohn E, Hiestand PC, Balatoni B, Reuschel R, Beerli C, Schwartz M, Billich A, 2007. Brain penetration of the oral immunomodulatory drug FTY720 and its phosphorylation in the central nervous system during experimental autoimmune encephalomyelitis: consequences for mode of action in multiple sclerosis. J. Pharmacol. Exp. Therapeut. 323, 469–475.

Author Manuscript Author Manuscript Author Manuscript Author Manuscript

Goncalves L, Dickenson AH, 2012. Asymmetric time-dependent activation of right central amygdala neurones in rats with peripheral neuropathy and pregabalin modulation. Eur. J. Neurosci. 36, 3204–3213. [PubMed: 22861166]

Haubensak W, Kunwar PS, Cai H, Ciocchi S, Wall NR, Ponnusamy R, Biag J, Dong HW, Deisseroth K, Callaway EM, Fanselow MS, Luthi A, Anderson DJ, 2010. Genetic dissection of an amygdala microcircuit that gates conditioned fear. Nature 468, 270–276. [PubMed: 21068836]

Hua T, Chen B, Lu D, Sakurai K, Zhao S, Han BX, Kim J, Yin L, Chen Y, Lu J, Wang F, 2020. General anesthetics activate a potent central pain-suppression circuit in the amygdala. Nat. Neurosci. 23, 854–868. [PubMed: 32424286]

Hunt S, Sun Y, Kucukdereli H, Klein R, Sah P, 2017. Intrinsic circuits in the lateral central amygdala. eNeuro 4.

Ji G, Neugebauer V, 2007. Differential effects of CRF1 and CRF2 receptor antagonists on pain-related sensitization of neurons in the central nucleus of the amygdala. J. Neurophysiol. 97, 3893–3904. [PubMed: 17392412]

Ji G, Horvath C, Neugebauer V, 2009. NR2B receptor blockade inhibits pain-related sensitization of amygdala neurons. Mol. Pain 5, 21. [PubMed: 19400952]

LeDoux JE, Iwata J, Cicchetti P, Reis DJ, 1988. Different projections of the central amygdaloid nucleus mediate autonomic and behavioral correlates of conditioned fear. J. Neurosci. 8, 2517–2529. [PubMed: 2854842]

Lee MJ, Van Brocklyn JR, Thangada S, Liu CH, Hand AR, Menzeleev R, Spiegel S, Hla T, 1998. Sphingosine-1-phosphate as a ligand for the G protein-coupled receptor EDG-1. Science 279, 1552–1555. [PubMed: 9488656]

Lein ES, Hawrylycz MJ, Ao N, Ayres M, Bensinger A, Bernard A, Boe AF, Boguski MS, Brockway KS, Byrnes EJ, Chen L, Chen L, Chen TM, Chin MC, Chong J, Crook BE, Czaplinska A, Dang CN, Datta S, Dee NR, Desaki AL, Desta T, Diep E, Dolbeare TA, Donelan MJ, Dong HW, Dougherty JG, Duncan BJ, Ebbert AJ, Eichele G, Estin LK, Faber C, Facer BA, Fields R, Fischer SR, Fliss TP, Frensley C, Gates SN, Glattfelder KJ, Halverson KR, Hart MR, Hohmann JG, Howell MP, Jeung DP, Johnson RA, Karr PT, Kawal R, Kidney JM, Knapik RH, Kuan CL, Lake JH, Laramee AR, Larsen KD, Lau C, Lemon TA, Liang AJ, Liu Y, Luong LT, Michaels J, Morgan JJ, Morgan RJ, Mortrud MT, Mosqueda NF, Ng LL, Ng R, Orta GJ, Overly CC, Pak TH, Parry SE, Pathak SD, Pearson OC, Puchalski RB, Riley ZL, Rockett HR, Rowland SA, Royall JJ, Ruiz MJ, Sarno NR, Schaffnit K, Shapovalova NV, Sivisay T, Slaughterbeck CR, Smith SC, Smith KA, Smith BI, Sodt AJ, Stewart NN, Stumpf KR, Sunkin SM, Sutram M, Tam A, Teemer CD, Thaller C, Thompson CL, Varnam LR, Visel A, Whitlock RM, Wohnoutka PE, Wolkey CK, Wong VY, Wood M, Yaylaoglu MB, Young RC, Youngstrom BL, Yuan XF, Zhang B, Zwingman TA, Jones AR, 2007. Genome-wide atlas of gene expression in the adult mouse brain. Nature 445, 168–176. [PubMed: 17151600]

Li W, Neugebauer V, 2004a. Block of NMDA and non-NMDA receptor activation results in reduced background and evoked activity of central amygdala neurons in a model of arthritic pain. Pain 110, 112–122. [PubMed: 15275758]

Li W, Neugebauer V, 2004b. Differential roles of mGluR1 and mGluR5 in brief and prolonged nociceptive processing in central amygdala neurons. J. Neurophysiol. 91, 13–24. [PubMed: 13679408]

Li JN, Sheets PL, 2018. The central amygdala to periaqueductal gray pathway comprises intrinsically distinct neurons differentially affected in a model of inflammatory pain. J. Physiol. 596, 6289–6305. [PubMed: 30281797]

Li H, Penzo MA, Taniguchi H, Kopec CD, Huang ZJ, Li B, 2013. Experience-dependent modification of a central amygdala fear circuit. Nat. Neurosci. 16, 332–339. [PubMed: 23354330]

Liu Y, Wada R, Yamashita T, Mi Y, Deng CX, Hobson JP, Rosenfeldt HM, Nava VE, Chae SS, Lee MJ, Liu CH, Hla T, Spiegel S, Proia RL, 2000. Edg-1, the G protein-coupled receptor for sphingosine-1-phosphate, is essential for vascular maturation. J. Clin. Invest. 106, 951–961. [PubMed: 11032855]

Marciniak A, Camp SM, Garcia JGN, Polt R, 2018a. An update on sphingosine-1-phosphate receptor 1 modulators. Bioorg. Med. Chem. Lett 28, 3585–3591. [PubMed: 30409535]

Author Manuscript Author Manuscript Author Manuscript Author Manuscript

Marciniak A, Camp SM, Garcia JGN, Polt R, 2018b. An update on sphingosine-1-phosphate receptor 1 modulators. Bioorg. Med. Chem. Lett 28, 3585–3591. [PubMed: 30409535]

McCall JG, Al-Hasani R, Siuda ER, Hong DY, Norris AJ, Ford CP, Bruchas MR, 2015. CRH engagement of the locus coeruleus noradrenergic system mediates stress-induced anxiety. Neuron 87, 605–620. [PubMed: 26212712]

Meyer zu Heringdorf D, Lass H, Kuchar I, Lipinski M, Alemany R, Rumenapp U, Jakobs KH, 2001. Stimulation of intracellular sphingosine-1-phosphate production by G-protein-coupled sphingosine-1-phosphate receptors. Eur. J. Pharmacol. 414, 145–154. [PubMed: 11239914]

Neugebauer V, 2015. Amygdala pain mechanisms. Handb. Exp. Pharmacol. 227, 261–284. [PubMed: 25846623]

Neugebauer V, Li W, 2003. Differential sensitization of amygdala neurons to afferent inputs in a model of arthritic pain. J. Neurophysiol. 89, 716–727. [PubMed: 12574449]

Nishimura H, Akiyama T, Irei I, Hamazaki S, Sadahira Y, 2010. Cellular localization of sphingosine-1-phosphate receptor 1 expression in the human central nervous system. J. Histochem. Cytochem. 58, 847–856. [PubMed: 20566754]

Okamoto H, Takuwa N, Gonda K, Okazaki H, Chang K, Yatomi Y, Shigematsu H, Takuwa Y, 1998. EDG1 is a functional sphingosine-1-phosphate receptor that is linked via a Gi/o to multiple signaling pathways, including phospholipase C activation, Ca2+ mobilization, Ras-mitogen-activated protein kinase activation, and adenylate cyclase inhibition. J. Biol. Chem. 273, 27104–27110. [PubMed: 9765227]

Penzo MA, Robert V, Li B, 2014. Fear conditioning potentiates synaptic transmission onto long-range projection neurons in the lateral subdivision of central amygdala. J. Neurosci. 34, 2432–2437. [PubMed: 24523533]

Qi Y, Mair N, Kummer KK, Leitner MG, Camprubi-Robles M, Langeslag M, Kress M, 2018. Identification of chloride channels CLCN3 and CLCN5 mediating the excitatory Cl(−) currents activated by sphingosine-1-phosphate in sensory neurons. Front. Mol. Neurosci. 11, 33. [PubMed: 29479306]

Quancard J, Bollbuck B, Janser P, Angst D, Berst F, Buehlmayer P, Streiff M, Beerli C, Brinkmann V, Guerini D, Smith PA, Seabrook TJ, Traebert M, Seuwen K, Hersperger R, Bruns C, Bassilana F, Bigaud M, 2012. A potent and selective S1P(1) antagonist with efficacy in experimental autoimmune encephalomyelitis. Chem. Biol. 19, 1142–1151. [PubMed: 22999882]

Riccio A, Li Y, Moon J, Kim KS, Smith KS, Rudolph U, Gapon S, Yao GL, Tsvetkov E, Rodig SJ, Van't Veer A, Meloni EG, Carlezon WA Jr., Bolshakov VY, Clapham DE, 2009. Essential role for TRPC5 in amygdala function and fear-related behavior. Cell 137, 761–772. [PubMed: 19450521]

Santini E, Porter JT, 2010. M-type potassium channels modulate the intrinsic excitability of infralimbic neurons and regulate fear expression and extinction. J. Neurosci. 30, 12379–12386. [PubMed: 20844133]

Schiess MC, Callahan PM, Zheng H, 1999. Characterization of the electrophysiological and morphological properties of rat central amygdala neurons in vitro. J. Neurosci. Res. 58, 663–673. [PubMed: 10561694]

Science A.I.f.B., 2006. Allen Mouse Brain ISH.

Selley DE, Welch SP, Sim-Selley LJ, 2013. Sphingosine lysolipids in the CNS: endogenous cannabinoid antagonists or a parallel pain modulatory system? Life Sci. 93, 187–193. [PubMed: 23782998]

Sim-Selley LJ, Goforth PB, Mba MU, Macdonald TL, Lynch KR, Milstien S, Spiegel S, Satin LS, Welch SP, Selley DE, 2009. Sphingosine-1-phosphate receptors mediate neuromodulatory functions in the CNS. J. Neurochem. 110, 1191–1202. [PubMed: 19493165]

Sim-Selley LJ, Wilkerson JL, Burston JJ, Hauser KF, McLane V, Welch SP, Lichtman AH, Selley DE, 2018. Differential tolerance to FTY720-induced antinociception in acute thermal and nerve injury mouse pain models: role of sphingosine-1-phosphate receptor adaptation. J. Pharmacol. Exp. Therapeut. 366, 509–518.

Sosulina L, Meis S, Seifert G, Steinhauser C, Pape HC, 2006. Classification of projection neurons and interneurons in the rat lateral amygdala based upon cluster analysis. Mol. Cell. Neurosci. 33, 57–67. [PubMed: 16861000]

Author Manuscript Author Manuscript Author Manuscript Author Manuscript

Strub GM, Maceyka M, Hait NC, Milstien S, Spiegel S, 2010. Extracellular and intracellular actions of sphingosine-1-phosphate. Adv. Exp. Med. Biol. 688, 141–155. [PubMed: 20919652]

Suh BC, Hille B, 2007. Regulation of KCNQ channels by manipulation of phosphoinositides. J. Physiol. 582, 911–916. [PubMed: 17412763]

Suter BA, O'Connor T, Iyer V, Petreanu LT, Hooks BM, Kiritani T, Svoboda K, Shepherd GM, 2010. Ephus: multipurpose data acquisition software for neuroscience experiments. Front. Neural Circ. 4, 100.

Suter BA, Migliore M, Shepherd GM, 2013. Intrinsic electrophysiology of mouse corticospinal neurons: a class-specific triad of spike-related properties. Cerebr. Cortex 23, 1965–1977.

Van Doorn R, Van Horssen J, Verzijl D, Witte M, Ronken E, Van Het Hof B, Lakeman K, Dijkstra CD, Van Der Valk P, Reijerkerk A, Alewijnse AE, Peters SL, De Vries HE, 2010. Sphingosine 1-phosphate receptor 1 and 3 are upregulated in multiple sclerosis lesions. Glia 58, 1465–1476. [PubMed: 20648639]

Waeber C, Chiu ML, 1999. In vitro autoradiographic visualization of guanosine-5'-O-(3-[35S]thio)triphosphate binding stimulated by sphingosine 1-phosphate and lysophosphatidic acid. J. Neurochem. 73, 1212–1221. [PubMed: 10461914]

Watanabe T, Shimazaki T, Oda Y, 2017. Coordinated expression of two types of low-threshold K(+) channels establishes unique single spiking of mauthner cells among segmentally homologous neurons in the zebrafish hindbrain. eNeuro 4.

Welch SP, Sim-Selley LJ, Selley DE, 2012. Sphingosine-1-phosphate receptors as emerging targets for treatment of pain. Biochem. Pharmacol. 84, 1551–1562. [PubMed: 22971335]

Wilson TD, Valdivia S, Khan A, Ahn HS, Adke AP, Martinez Gonzalez S, Sugimura YK, Carrasquillo Y, 2019. Dual and opposing functions of the central amygdala in the modulation of pain. Cell Rep. 29, 332–346 e335. [PubMed: 31597095]

Xu SZ, Muraki K, Zeng F, Li J, Sukumar P, Shah S, Dedman AM, Flemming PK, McHugh D, Naylor J, Cheong A, Bateson AN, Munsch CM, Porter KE, Beech DJ, 2006. A sphingosine-1-phosphate-activated calcium channel controlling vascular smooth muscle cell motility. Circ. Res. 98, 1381–1389. [PubMed: 16675717]

Yanagida K, Liu CH, Faraco G, Galvani S, Smith HK, Burg N, Anrather J, Sanchez T, Iadecola C, Hla T, 2017. Size-selective opening of the blood-brain barrier by targeting endothelial sphingosine 1-phosphate receptor 1. Proc. Natl. Acad. Sci. U. S. A. 114, 4531–4536. [PubMed: 28396408]

Author Manuscript Author Manuscript Author Manuscript Author Manuscript

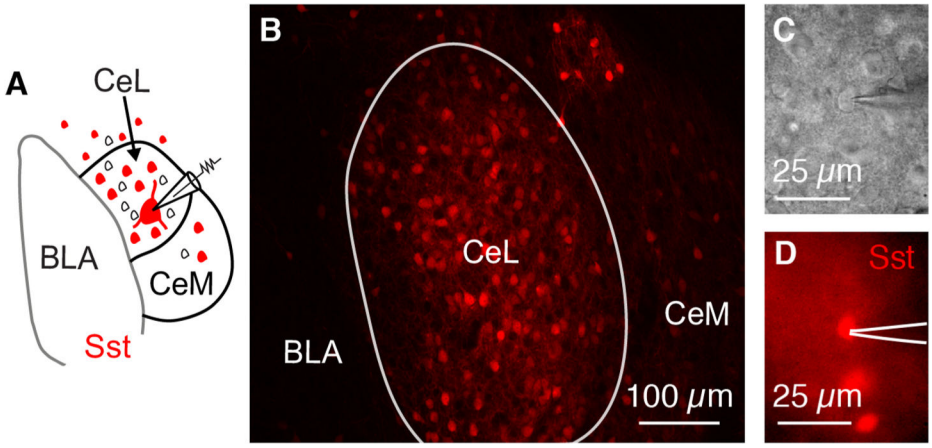

Fig. 1.

Identifying Sst neurons in the CeL for whole-cell electrophysiology. **A,** schematic depicting whole-cell patch-clamp recording from CeL, Sst neurons. **B,** fluorescent image **(4x)** depicting tdTomato-expressing Sst neurons in the CeL. **C,** bright field and **D,** fluorescent images (**60x**) showing whole cell recording of a Sst neuron in the CeL.

Author Manuscript Author Manuscript Author Manuscript Author Manuscript

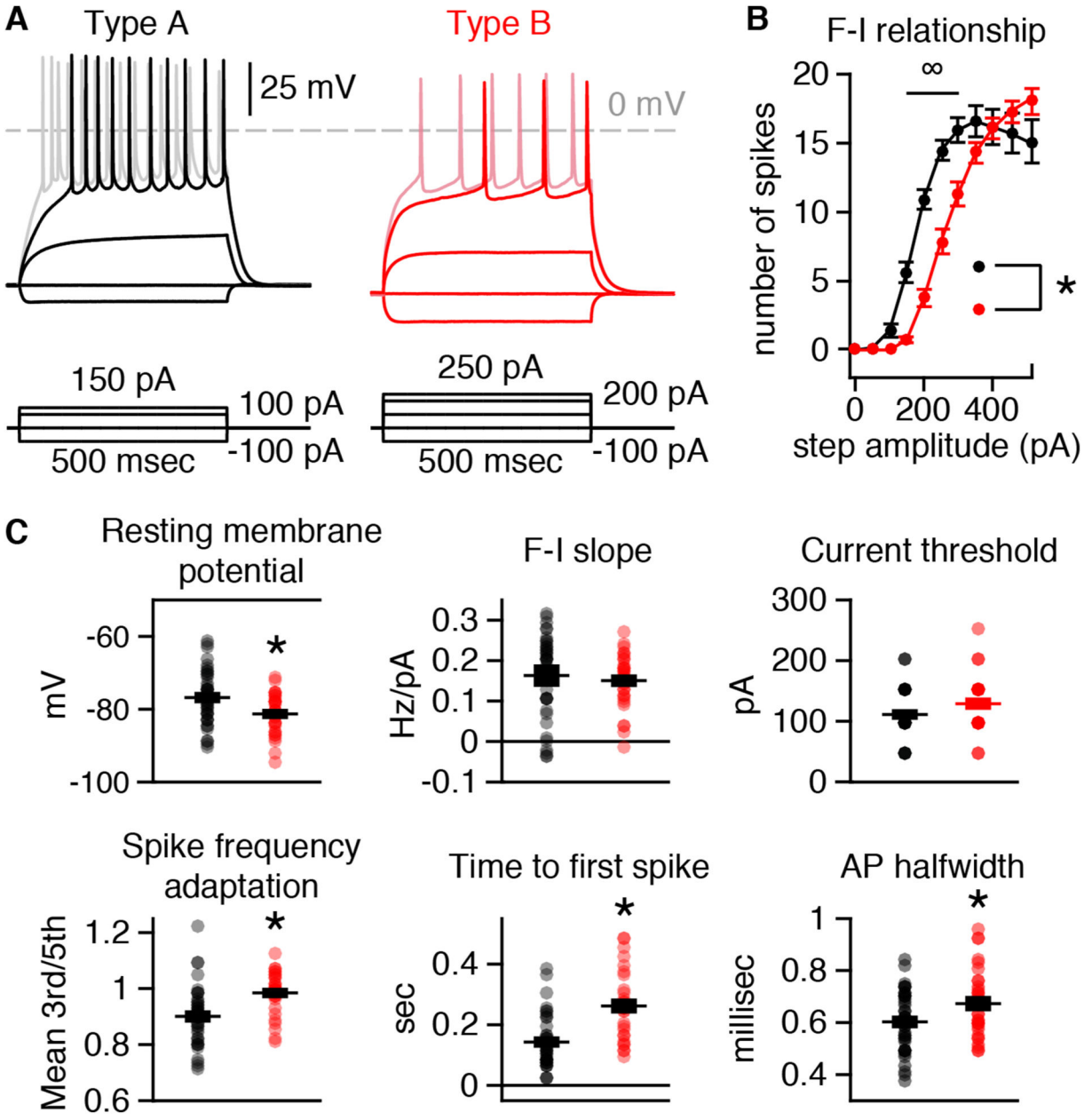

Fig. 2.

CeL Sst neurons consist of two electrophysiologically distinct subtypes. **A**, representative current-clamp traces of type A (black, left) and type B (red, right) CeL Sst neurons evoked by 500 msec current steps (bottom). **B,** number of action potentials in response to injected current in type A and type B neurons (41 type A cells (17M:24F) and 31 type B cells (18M:13F)) (2-way ANOVA of cell type $F(1,910) = 30.95$, *$p < 0.0001$; cell type × current interaction $F(12,910) = 7.572$, $p < 0.0001$ with multiple comparisons ∞$p < 0.05$). Data points indicate mean ± SEM. **C**, plots displaying comparisons of resting membrane potential (type A: −76.8 ± 1.15 mV; type B: −81.3 ± 1.01 mV), F-I slope (type A: 0.163 ± 0.016 Hz/pA; type B: 0.150 ± 0.012 Hz/pA), current threshold (type A median: 100 pA; type B median: 150 pA), spike frequency adaptation (type A: 0.901 ± 0.017; type B: 0.984 ±

Author Manuscript Author Manuscript Author Manuscript Author Manuscript

0.013), time to first spike (type A: 0.143 ± 0.014 s; type B: 0.262 ± 0.020 s), AP half-width (type A: 0.603 ± 0.018 msec; type B: 0.673 ± 0.024 msec). Data points are partially transparent, with less transparency indicating increased density of data clustering. Black box plots represent mean ± SEM. *P < 0.05.

Author Manuscript Author Manuscript Author Manuscript Author Manuscript

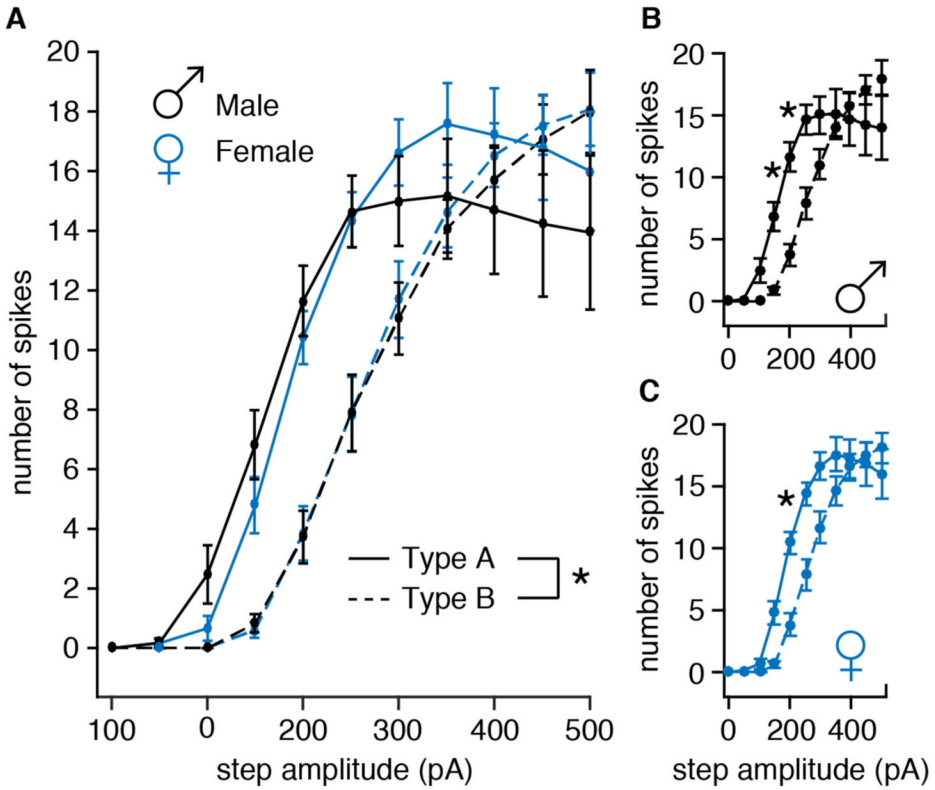

Fig. 3.

CeL Sst subtypes exhibit distinct excitability in both male and female mice. **A,** number of action potentials in response to injected current in type A (solid) and type B (dashed), male (black) and female (blue) neurons (41 type A cells (17M:24F) and 31 type B cells (18M:13F)) (3-way ANOVA of cell type $F(1,68) = 6.253$, *$p = 0.0148$; sex $F(1,68) = 0.2158$, $p = 0.6438$; current x cell type interaction $F(12, 816) = 10.73$, $p < 0.0001$). Excitability is altered in male **B** and female **C** mice (3-way ANOVA with multiple comparisons *$p < 0.05$). Data points indicate mean ± SEM.

Author Manuscript Author Manuscript Author Manuscript Author Manuscript

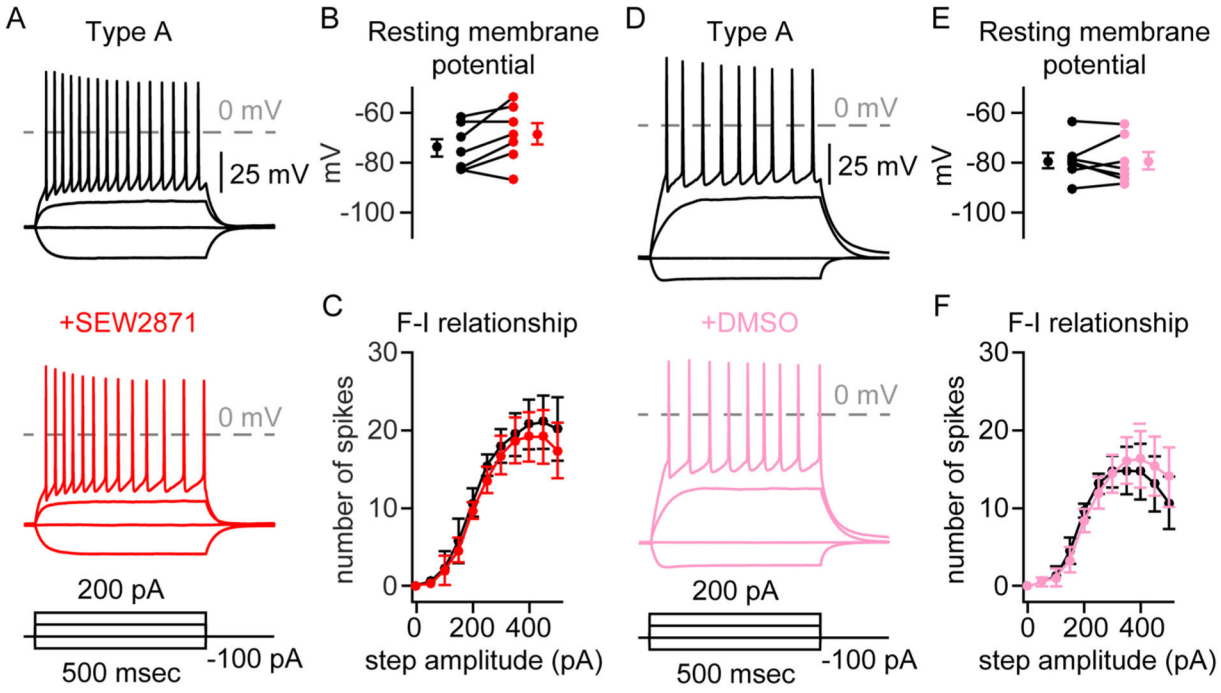

Fig. 4.

$S1PR_1$ agonist SEW2871 does not alter resting membrane potential or firing of type A Sst CeL neurons. **A,** current-clamp recording from a type A Sst CeL neuron before (black, top) and after 10-min application of SEW2871 (red, bottom). **B,** plot showing that SEW2871 has no effect on resting membrane potential of type A Sst CeL neurons. **C,** number of action potentials in response to injected current is unaltered after application of SEW2871 (n = 7 cells, 2-way ANOVA of drug $F(1,6) = 4.00$, $p = 0.092$; drug x current $F(12,72) = 0.615$, $p = 0.823$). **D,** current-clamp recording from a type A Sst CeL neuron before (black, top) and after 10-min application of the vehicle control DMSO (pink, bottom). **E, F** plots showing there is no effect of DMSO on **E** resting membrane potential however there is an effect on **F** number of action potentials in response to injected current (n = 7 cells, 2-way ANOVA of drug $F(1,6) = 0.364$, $p = 0.568$; drug x current $F(12,72) = 2.51$, $p = 0.008$). Sidak's multiple comparisons significance $p < 0.05$ indicated by *****. Data points indicate mean ± SEM.

Author Manuscript Author Manuscript Author Manuscript Author Manuscript

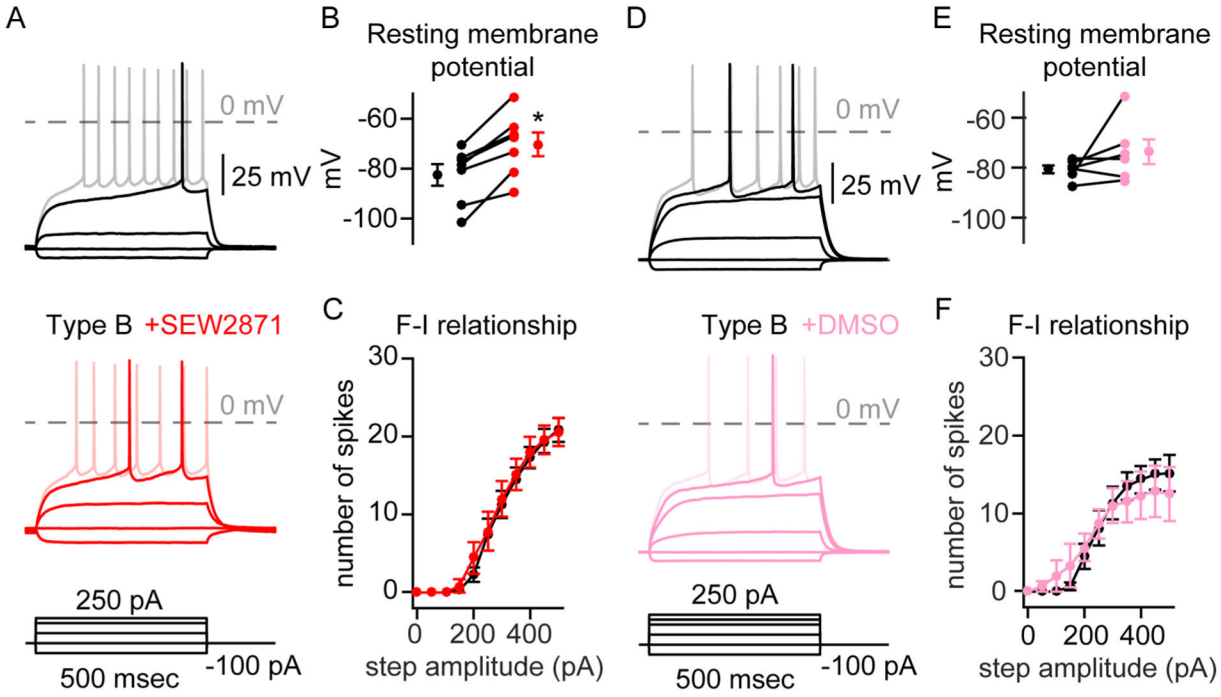

Fig. 5.

$S1PR_1$ agonist SEW2871 depolarizes resting membrane potential, but has no effect on firing, of type B Sst CeL neurons. **A,** current-clamp recordings from a type B Sst CeL neuron before (black, top) and after 10-min application of SEW2871 (red, bottom). **B,** plot showing that SEW2871 significantly depolarizes resting membrane potential of type B Sst CeL neurons. **C,** number of action potentials in response to injected current is unaltered after application of SEW2871 (n = 7 cells, 2-way ANOVA of drug $F(1,6) = 0.280$, $p = 0.616$; drug x current $F(12,72) = 0.622$, $p = 0.817$). **D,** current-clamp recording from a type B Sst CeL neuron before (black, top) and after 10-min application of the vehicle control DMSO (pink, bottom). **E-F,** plots showing there is no effect of DMSO on **E** resting membrane potential, and **F** number of action potentials in response to injected current (n = 6 cells, 2-way ANOVA of drug $F(1,5) = 0.235$, $p = 0.648$; drug x current $F(12,60) = 0.919$, $p = 0.534$). Data points indicate mean ± SEM.

Author Manuscript Author Manuscript Author Manuscript Author Manuscript

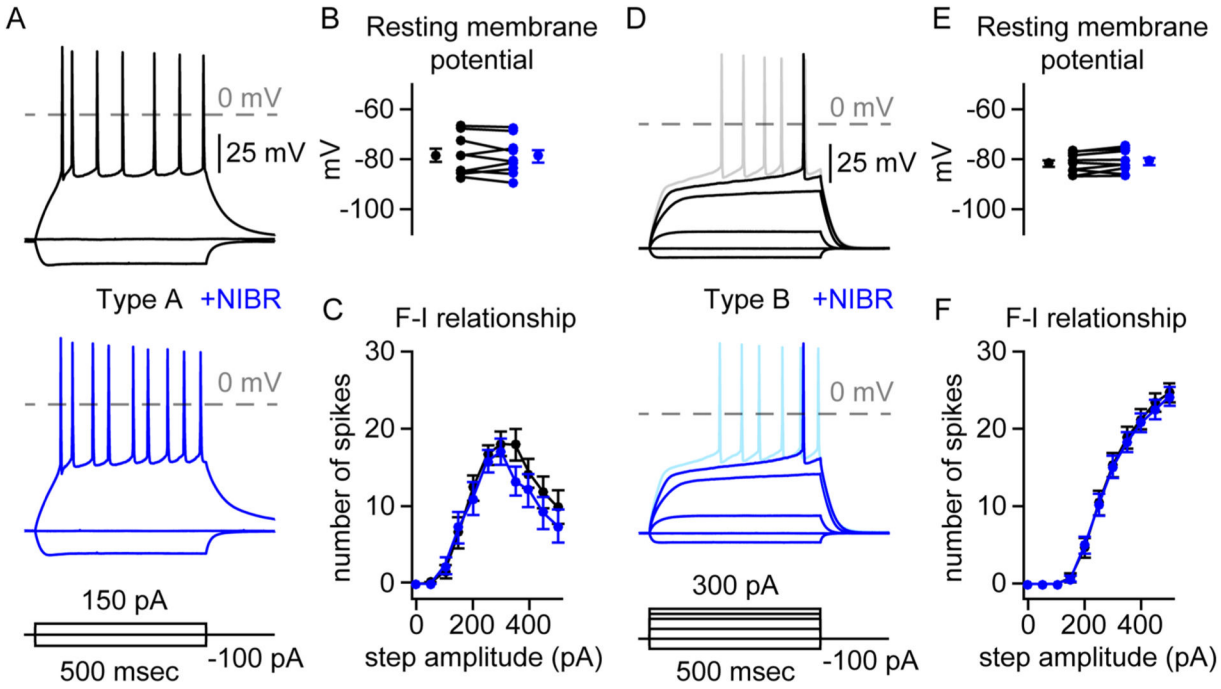

Fig. 6.

S1PR1 competitive antagonist NIBR has no effect on resting membrane potential or AP firing of Sst-neuron subtypes. **A,** current-clamp recordings from type A Sst CeL neurons before (black, top) and after 10-min application of NIBR (blue, bottom). **B-C,** plots showing there is no effect of NIBR on type A Sst CeL neuron **B** resting membrane potential and **C** number of action potentials in response to injected current (n = 7 cells, 2-way ANOVA of drug $F(1,6) = 5.76$, $p = 0.053$; drug x current $F(2.32,13.9) = 2.50$, $p = 0.113$). **D,** current-clamp recording from a type B Sst CeL neuron before (black, top) and after 10-min application of NIBR (blue, bottom). **E-F,** plots showing there is no effect of NIBR on type B Sst CeL neuron **E** resting membrane potential, and **F** number of action potentials in response to injected current (n = 9 cells, 2-way ANOVA of drug $F(1,8) = 0.298$, $p = 0.600$; drug x current $F(1.77,14.2) = 0.726$, $p = 0.485$). Data points indicate mean ± SEM.

Author Manuscript Author Manuscript Author Manuscript Author Manuscript

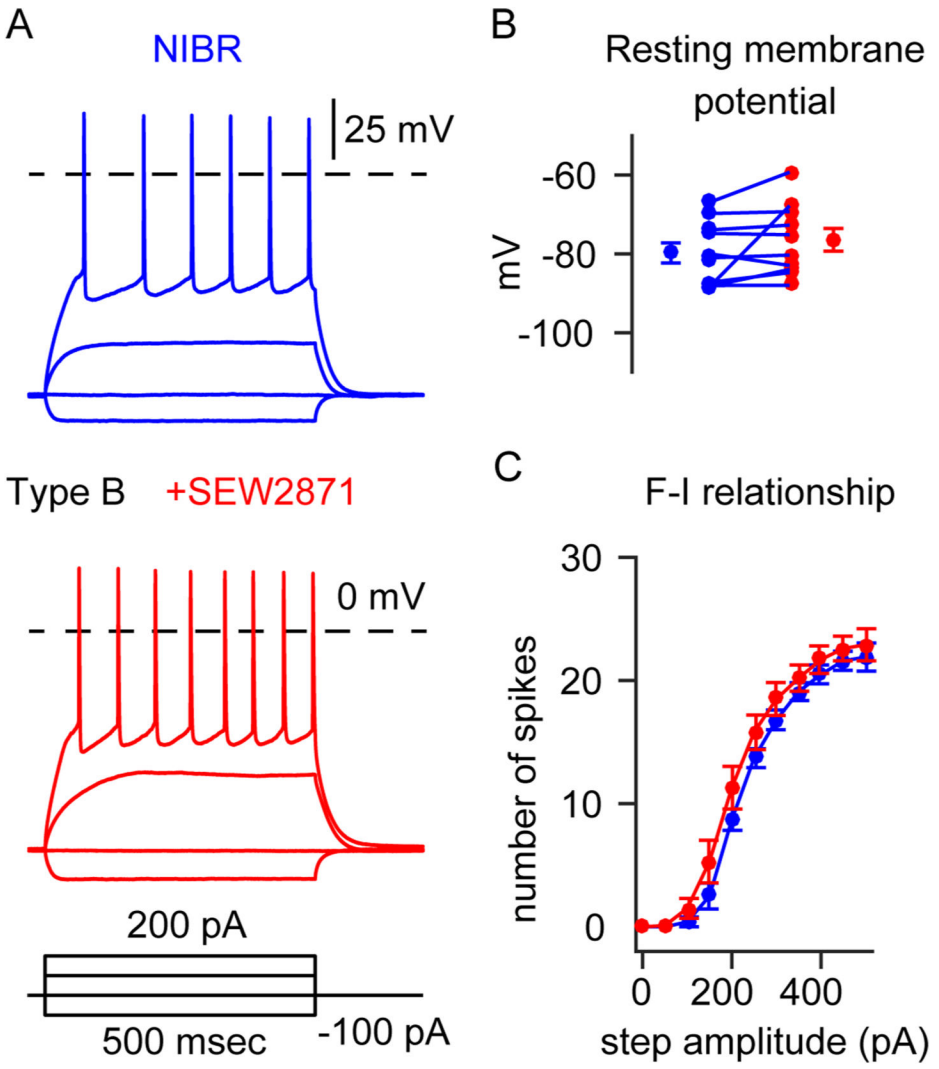

Fig. 7.

Bath exposure to NIBR blocks effect of SEW2871 effect on type B CeL Sst neurons. **A,** current-clamp recording from a type B CeL Sst neuron bathed in N1BR (100 nM) before (blue, top) and after 10-min application of SEW2871 (red, bottom). **B,** plot showing that SEW2871 has no effect on resting membrane potential of type B CeL Sst neuron bathed in N1BR (n = 10 cells, student's paired *t*-test t = 1.62, p = 0.140). **C,** number of action potentials in response to injected current is unaltered after application of SEW2871 (n = 10 cells, 2-way ANOVA of drug F(1,9) = 4.72, p = 0.0579; drug x current F(1.74,15.7) = 1.91, p = 0.184). Data points indicate mean ± SEM.

Author Manuscript Author Manuscript Author Manuscript Author Manuscript

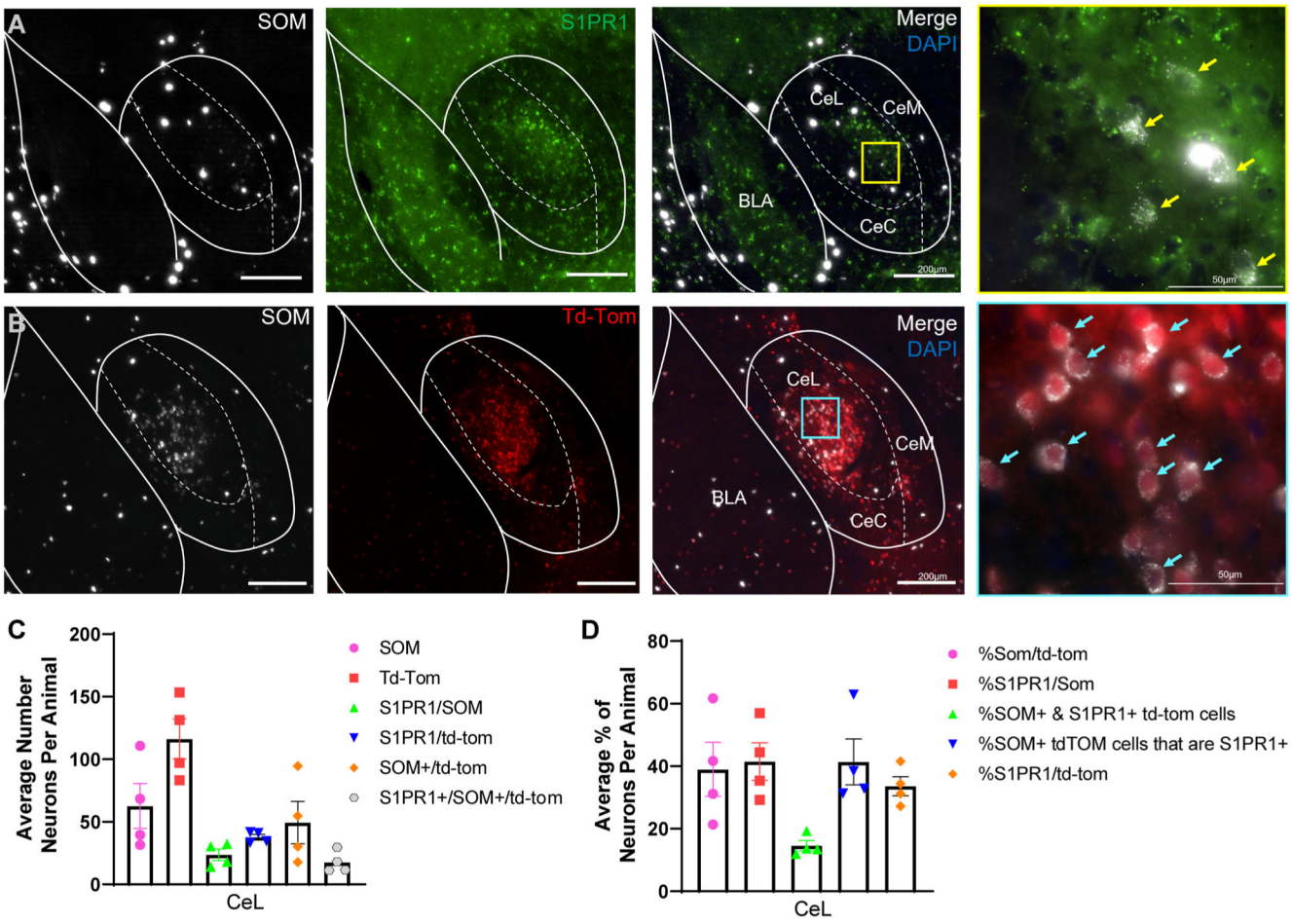

Fig. 8.

Quantification of fluorescence *in situ* hybridization from right CeA of Sst-tdTom mice **A,** Localization of Sst (**white**), $S1PR_1$ (**green**), and (20X) colocalization within the CeL (Sst, $S1PR_1$, DAPI) with 100X merge image with showing colocalization of Sst and $S1PR_1$ denoted by yellow arrows. **B,** Localization of Sst (**white**), Td-Tom (**red**), and (20X) colocalization within the CeL (Sst, Td-Tom, DAPI) with 100X merge image showing colocalization of Sst and Td-Tom denoted by cyan arrows. Scale bars = 200 μm, left and middle panels; scale bars = 50 μm, right panels. **C,** Average number and **D,** average % of neurons (One-way ANOVA: $F(4, 12) = 3.229$; $P = 0.0513$) detected per animal in CeL. N = 4 animals (2M; 2F), 4–5 slices per animal.

Author Manuscript Author Manuscript Author Manuscript Author Manuscript

Table 1

Intrinsic properties of Sst CeL neuronal subtypes by sex.

	Male		Female		
Sub-threshold properties	**Type A (n = 17)**	**Type B (n = 24)**	**Type A (n = 18)**	**Type B (n = 13)**	
Resting potential (mV)	− 77.7 ± 1.55	− 82.5 ± 1.34	− 76.2 ± 1.65	− 79.6 ± 1.48	F_{int} = 0.201 p = 0.655 F_{sex} = 1.83 p = 0.181 **F_{cell} = 6.62 p = 0.012**
Input Resistance (MΩ)	158 ± 8.02	144 ± 9.58	152 ± 9.15	137 ± 8.82	F_{int} = 3.80e^{-4} p = 0.985 F_{sex} = 0.469 p = 0.496 F_{cell} = 2.37 p = 0.129
Firing properties					
Current Threshold (pA)	100 †	100 †	100 †	150 †	F_{int} = 0.224 p = 0.639 F_{sex} = 3.39 p = 0.070 **F_{cell} = 4.51 p = 0.038**
Voltage Threshold (mV)	− 34.7 ± 1.44	− 32.5 ± 1.09	− 32.0 ± 1.18	− 28.3 ± 1.92	F_{int} = 0.271 p = 0.605 **F_{sex} = 6.10 p = 0.016** **F_{cell} = 4.52 p = 0.037**
AP half-width (seconds)	58.0 ± 2.72 e^{-5}	65.4 ± 3.10 e^{-5}	61.8 ± 2.44 e^{-5}	70.0 ± 3.71 e^{-5}	F_{int} = 0.150 p = 0.700 F_{sex} = 1.87 p = 0.177 **F_{cell} = 7.33 p = 0.009**
Frequency-current slope (Hz/pA)	0.142 ± 0.028	0.148 ± 0.017	0.177 ± 0.019	0.153 ± 0.017	F_{int} = 0.483 p = 0.490 F_{sex} = 0.812 p = 0.371 F_{cell} = 0.172 p = 0.680
Time to first AP (seconds)	0.120 ± 0.015	0.281 ± 0.024	0.158 ± 0.020	0.235 ± 0.033	F_{int} = 3.23 p = 0.077 F_{sex} = 0.036 p = 0.849 **F_{cell} = 25.4 p < 0.0001**
Height (mV)	73.2 ± 2.50	71.4 ± 2.34	72.8 ± 1.63	66.7 ± 1.85	F_{int} = 1.02 p = 0.316 F_{sex} = 1.39 p = 0.242 F_{cell} = 3.45 p = 0.068
Spike-frequency adaptation (mean 5th/10th)	0.925 ± 0.021	0.981 ± 0.017	0.902 ± 0.015	0.987 ± 0.014	F_{int} = 1.21 p = 0.276 F_{sex} = 1.80 p = 0.184 **F_{cell} = 4.62 p = 0.035**
Fast after-hyperpolarization (mV)	− 7.40 ± 1.09	− 9.63 ± 1.82	− 7.56 ± 0.645	− 8.86 ± 0.965	F_{int} = 0.144 p = 0.706 F_{sex} = 0.062 p = 0.804 F_{cell} = 2.06 p = 0.156

Resting membrane potential evaluated with no applied current, all other properties evaluated with current applied to hold the membrane potential near minus 70 mV. Data presented as mean ± SEM

† median, n is the number of cells. 3-way ANOVA F-statistics (df = 1, 67): F_{int} – interaction; F_{sex} – effect of sex; F_{cell} – effect of cell type, are presented in the final column with significant results bolded (p < 0.05). n = 51 mice (23M:28F), 41 Type A cells (17M:24F) and 31 Type B cells (18M:13F). Age of mice: average, 52; median, 48.

Author Manuscript Author Manuscript Author Manuscript Author Manuscript

Neuropharmacology. Author manuscript; available in PMC 2022 February 01.

Table 2

Effect of $S1PR_1$ pharmacology on intrinsic properties of Sst CeL Type A and Type B neurons.

	SEW2871			**DMSO**			**NIBR**		
Sub-threshold properties	***Type A (n = 7)***	***Type B (n = 7)***		***Type A (n = 7)***	**Type B (n = 6)**		***Type A (n = 7)***	***Type B (n = 9)***	
Resting potential (mV)	− 73.9 ± 3.5 − 68.3 ± 4.3	− 82.6 ± 4.3 − 70.3 ± 4.8**Δ**	F(1,12) = 3.93 p = 0.07 **F_{SEW} = 28.7 p = 2.0e^{-4}** F_{cell} = 0.863 p = 0.37	− 79.1 ± 3.07 − 79.2 ± 3.49	− 80.7 ± 1.6 − 73.7 ± 5.0	F(1,11) = 1.98 p = 0.19 F_{DMSO} = 1.86 p = 0.20 F_{cell} = 0.222 p = 0.65	− 78.5 ± 3.4 − 79.0 ± 3.2	− 81.8 ± 1.3 − 80.9 ± 1.4	F(1,14) = 0.639 p = 0.44 F_{NIBR} = 0.060 p = 0.81 F_{cell} = 0.639 p = 0.44
Input Resistance (MΩ)	131 ± 28.1 159 ± 19.5	118 ± 36.3 159 ± 39.9**Δ**	F(1,12) = 0.468 p = 0.51 **F_{SEW} = 12.4 p = 0.004** F_{cell} = 0.027 p = 0.87	170 ± 21.7 163 ± 24.0	117 ± 5.41 127 ± 7.43	**F**(1,11) = 2.22 p = 0.16 F_{DMSO} = 0.067 p = 0.80 F_{cell} = 3.19 p = 0.10	158 ± 20.4 158 ± 20.6	131 ± 15.2 133 ± 13.0	F(1,14) = 0.053 p = 0.82 F_{NIBR} = 0.182 p = 0.68 F_{cell} = 1.19 p = 0.29
Firing properties									
Current Threshold (pA)	150 *†* 150 *†*	200 *†* 200 *†*	F(1,12) = 1.80 p = 0.21 F_{SEW} = 0.200 p = 0.66 **F_{cell} = 6.94 p = 0.02**	150 *†* 150 *†*	200 *†* 200 *†*	F(1,11) = 1.42 p = 0.26 F_{DMSO} = 0.438 p = 0.52 F_{cell} = 1.41 p = 0.260	150 *†* 100 *†*	200 *†* 200 *†*	F(1,14) = 0.236 p = 0.64 F_{NIBR} = 0.236 p = 0.64 **F_{cell} = 12.2 p = 0.004**
Voltage Threshold (mV)	− 33.3 ± 0.634 − 28.1 ± 2.20	− 32.2 ± 1.9 − 25.3 ± 2.1**Δ**	F(1,12) = 0.343 p = 0.57 **F_{SEW} = 15.8 p = 0.002** F_{cell} = 0.860 p = 0.37	− 33.5 ± 1.70 − 34.4 ± 1.97	− 30.6 ± 3.24 − 30.9 ± 4.34	F(1,11) = 0.169 p = 0.69 F_{DMSO} = 0.538 p = 0.48 F_{cell} = 0.651 p = 0.44	− 39.5 ± 3.2 − 39.8 ± 2.8	− 34.8 ± 1.4 − 34.0 ± 1.8	F(1,14) = 0.604 p = 0.45 F_{NIBR} = 0.097 p = 0.76 F_{cell} = 2.87 p = 0.112
AP half-width (seconds)	50.2 ± 2.3 e^{-5} 50.9 ± 3.1e^{-5}	66.7 ± 9.9 e^{-5} 59.8 ± 3.8 e^{-5}	F(1,12) = 0.85 p = 0.38 F_{SEW} = 0.577 p = 0.46 F_{cell} = 3.40 p = 0.090	60.5 ± 4.61 e^{-5} 57.7 ± 4.25 e^{-5}	65.8 ± 5.1e^{-5} 65.5 ± 6.2 e^{-5}	F(1,11) = 1.12 p = 0.31 F_{DMSO} = 1.61 p = 0.23 F_{cell} = 0.88 p = 0.37	50.2 ± 3.7 e^{-5} 52.1 ± 5.4 e^{-5}	54.7 ± 2.1 e^{-5} 54.8 ± 2.1 e^{-5}	F(1,14) = 0.295 p = 0.60 F_{NIBR} = 0.363 p = 0.56 F_{cell} = 0.650 p = 0.43
Frequency-current slope (Hz/ pA)	0.21 ± 0.02 0.21 ± 0.02	0.15 ± 0.01 0.15 ± 0.02	F(1,12) = 0.327 p = 0.58 F_{SEW} = 0.064 p = 0.81 **F_{cell} = 6.43 p = 0.03**	0.053 ± 0.02 0.072 ± 0.03	0.095 ± 0.01 0.112 ± 0.03	F(1,11) = 0.006 p = 0.94 F_{DMSO} = 2.39 p = 0.15 F_{cell} = 1.55 p = 0.24	0.039 ± 0.01 0.015 ± 0.02**Δ**	0.168 ± 0.009 0.164 ± 0.010	F(1,14) = 2.62 p = 0.13 **F_{NIBR} = 5.40 p = 0.036** **F_{cell} = 74.9 p < 1 e^{-4}**
Time to First AP (seconds)	0.13 ± 0.04 0.14 ± 0.03	0.311 ± 0.04 0.191 ± 0.05**Δ**	F(1,12) = 4.71 p = 0.05 F_{SEW} = 3.29 p = 0.095 **F_{cell} = 6.04 p = 0.03**	0.130 ± 0.04 0.158 ± 0.03	0.308 ± 0.02 0.248 ± 0.04	F(1,11) = 1.99 p = 0.19 F_{DMSO} = 0.269 p = 0.61 **F_{cell} = 12.7 p = 0.004**	0.089 ± 0.02 0.109 ± 0.04	0.267 ± 0.03 0.274 ± 0.04	F(1,14) = 0.047 p = 0.83 F_{NIBR} = 0.196 p = 0.67 **F_{cell} = 18.0 p = 0.0008**
Height (mV)	76.6 ± 2.04 74.7 ± 2.68	73.7 ± 4.11 68.4 ± 5.35**Δ**	F(1,12) = 1.95 p = 0.19 **F_{SEW} = 9.06 p = 0.01** F_{cell} = 0.784 p = 0.39	72.8 ± 3.2 69.8 ± 3.0	70.7 ± 2.4 69.1 ± 3.4	F(1,11) = 0.462 p = 0.51 F_{DMSO} = 4.39 p = 0.06 F_{cell} = 0.109 p = 0.75	82.5 ± 6.8 78.2 ± 3.7	73.6 ± 2.8 70.1 ± 3.8	F(1,14) = 0.028 p = 0.87 F_{NIBR} = 2.64 p = 0.13 F_{cell} = 2.32 p = 0.15
Spike-frequency adaptation (mean 5th/10th)	2.34 ± 1.42 0.91 ± 0.03	0.994 ± 0.05 0.951 ± 0.03	F(1,12) = 0.963 p = 0.35 F_{SEW} = 1.09 p = 0.32 F_{cell} = 0.834 p = 0.38	0.941 ± 0.05 0.926 ± 0.05	1.01 ± 0.03 0.90 ± 0.04**Δ**	**F(1,11) = 5.68 p = 0.04** **F_{DMSO} = 9.87 p = 0.009** F_{cell} = 0.103 p = 0.76	0.846 ± 0.04 0.882 ± 0.02	1.03 ± 0.01 1.02 ± 0.02	F(1,14) = 2.78 p = 0.12 F_{NIBR} = 0.744 p = 0.40 **F_{cell} = 27.6 p = 0.0001**
Fast after-hyperpolarization (mV)	− 6.59 ± 0.750	− 6.49 ± 1.44	F(1,11) = 1.01 p = 0.34 F_{SEW} = 1.52 p = 0.24 F_{cell} = 0.502 p = 0.50	− 9.92 ± 1.6 − 9.59 ± 1.4	− 3.59 ± 1.5 − 4.74 ± 1.6	F(1,11) = 1.57 p = 0.24 F_{DMSO} = 0.473 p = 0.51 **F_{cell} = 7.28 p = 0.021**	− 6.71 ± 1.3 − 5.42 ± 1.3	− 7.35 ± 0.98	F(1,14) = 1.97 p = 0.18 F_{NIBR} = 0.704 p = 0.42 F_{cell} = 0.951 p = 0.35

Author Manuscript Author Manuscript Author Manuscript Author Manuscript

	SEW2871			DMSO			NIBR		
Sub-threshold properties	***Type A (n = 7)***	***Type B (n = 7)***		***Type A (n = 7)***	**Type B (n = 6)**		***Type A (n = 7)***	***Type B (n = 9)***	
	− 8.22 ± 0.332	− 6.66 ± 1.02						− 7.68 ± 1.01	

Mixed-effects analysis (pre-drug vs. drug, Type A vs. Type B) is presented in the column right-adjacent to pharmacology with significant results **bolded** ($p < 0.05$); F(DFn, DFd), Fixed effect of cell type x drug treatment; DFn, degrees Freedom For numerator; DFd, degrees Freedom For denominator; F_{drug}, Fixed effect of drug treatment; F_{cell}, Fixed effect of cell type. Multiple comparisons significance $p < 0.05$ indicated by **Δ** Following treated cell in corresponding cell type. n = 27 mice (12M:15F), 14 SEW2871 treated cells (5M:9F), 13 DMSO treated cells (6M:7F), and 16 NIBR treated cells (8M:7F). Age of mice: average, 50; median, 48. Data presented as mean ± SEM

†= median, n is the number of cells recorded.

Author Manuscript

Author Manuscript

Author Manuscript

Author Manuscript

Table 3

Pharmacological effect of SEW2871 on Sst CeL type B neuron intrinsics pre-exposed to NIBR.

	Type B		
Sub-threshold properties	**NIBR baseline**	**SEW2871**	
Resting potential (mV)	− 79.8 ± 2.56	− 76.4 ± 2.89	p = 0.140 t = − 1.62 df = 9
Input Resistance (MΩ)	165 ± 20.4	175 ± 17.8	p = 0.410 t = − 0.865 df = 9
Firing properties			
Current Threshold (pA)	150 †	150 †	p = 0.343 t = 1 df = 9
Voltage Threshold (mV)	− 35.7 ± 1.37	−36.6 ± 1.27	p = 0.474 t = 0.745 df = 9
AP half-width (seconds)	62.5 ± 2.32 e− 5	62.8 ± 3.44 e− 5	p = 0.896 t = − 0.134 df = 9
Frequency-current slope (Hz/pA)	0.174 ± 0.009	0.187 ± 0.012	p = 0.290 t = − 1.13 df = 9
Time to first AP (seconds)	0.225 ± 0.05	0.213 ± 0.03	p = 0.855 t = 0.188 df = 9
Height (mV)	72.0 ± 2.66	68.6 ± 2.99	p = 0.896 t = − 0.134 df = 9
Spike-frequency adaptation (mean 5th/10th)	0.988 ± 0.03	0.982 ± 0.03	p = 0.817 t = 0.238 df = 9
Fast after-hyperpolarization (mV)	− 5.81 ± 1.11	− 7.40 ± 1.07	p = 0.182 t = 1.45 df = 9

All properties evaluated with no applied current, at resting membrane potential. Data presented as mean ± SEM

†median. Paired *t*-test significance by cell type indicated by bold ($p < 0.05$). n = 6 mice (3M:3F; average postnatal day, 50; median postnatal day, 50), 10 Type B cells (5M:5F).